Performance Improvement of a Direct Carbon Fuel Cell through an Irreversible Vacuum Thermionic Generator

Yuan Wang(王远)[1] and Shanhe Su(苏山河)[2*]

[1]*Henan Engineering Technology Research Center of Energy Conversion and Storage Materials, Henan University of Engineering, Zhengzhou 451191, China*
[2]*Department of Physics, Xiamen University, Xiamen 361005, China*

(Received 30 July 2023; accepted manuscript online 15 November 2023)

A novel hybrid system consisting of a direct carbon fuel cell (DCFC), a thermionic generator (TIG), and a regenerator is developed to recover the exhaust heat from the fuel cell. Expressions for the power output and efficiency of subsystems and the hybrid system are derived. Based on the energy balance equation, the area matching problem between the DCFC and the TIG is discussed and solved. By considering the main irreversibilities, the influences of the DCFC's current density and the TIG's voltage on the performance of the hybrid system are revealed. The maximum power output density and the corresponding efficiency of the hybrid system are, respectively, equal to 379 $\mathrm{W/m^2}$ and 36%. To enhance the maximum power density of the single DCFC, the optimal regions of the main parameters are determined.

DOI: 10.1088/0256-307X/40/12/128201

Direct carbon fuel cells (DCFCs) can directly convert the carbon energy into electricity by using the solid carbon as fuel, such as refuse fuel, biomass, and coal.[1,2] As a special type of high temperature fuel cell, DCFCs offer higher efficiency and lower CO_2 emission[3,4] and are broadly classified into solid oxide DCFCs,[5–7] molten carbonate DCFCs,[8,9] and molten hydroxide DCFCs,[10,11] among which the molten carbonate DCFCs have the advantages of high conductivity, suitable melting temperature, and long-term stability in CO_2, and are attracting ever increasing interests.[12]

Investigations using experimental tests,[13–18] theoretical modeling, and simulations on the inner irreversibilities of DCFCs have been carried out by many researchers to improve the maximum power density.[19–21] Liu *et al.*[22] simulated the performance of a direct carbon fuel cell, adopted an improved packed bed anode, and took the electrochemical reaction dynamics, mass-transfer, and electrode processes into account. In the temperature range 923–1023 K, the results obtained have shown that the anode activation polarization is the major potential loss. Eom *et al.*[23] modeled the activation and ohmic polarization losses by considering the correlation between the surface properties and inner resistance. Xu *et al.*[24] proposed a 2D model for direct carbon solid oxide fuel cells, in which performances of the H_2O agent and CO_2 agent for carbon gasification were compared. To improve the maximum power density, integrating the fuel cells with other kinds of power plants is an alternative method. Steinberg[25] proposed an integrated plasma fuel cell, which combines a hydrogen plasma black reactor and a molten carbonate DCFC to convert fossil and biomass fuels with a thermal efficiency of producing hydrogen and electricity varying from 70 to 90%. Zhang *et al.*[26] gave a packed bed anode DCFC model, which uses molten carbonate as an electrolyte and graphite as a fuel. The analytical expressions of the activation overpotentials, ohmic overpotentials, and concentration overpotentials are derived. Due to high operating temperatures, several studies have been performed on fuel cell-heat engine hybrid systems to recover the high-quality exhaust heat of the fuel cell.[27,28] In the DCFC, most parts of the chemical energy during the reaction will be finally released as waste heat due to the internal resistance. Hybrid direct carbon fuel cells (HDCFCs) are promising to achieve high power density, good fuel-electrode contact, and high carbon-fuel conversion efficiency due to increased reaction sites and hybrid routines of carbon utilization.[29] One of the possible heat engines that can be used as the bottom system of the DCFC is the thermionic generator (TIG).[30] The application of the TIG as a subsystem has been proposed in high temperature fuel cells, such as the solid oxide fuel cell[31] and the molten carbonate fuel cell.[32] Traditional metal-based TIGs usually have a large work function and require an extremely high operating temperature.[33] This may increase the temperature difference between two electrodes, leading to large irreversible thermodynamic losses during the electron and heat transports. In addition, the output voltage depends on the difference between the cathode and anode work functions. Lower cathode work function will result in lower voltage.[34] The output voltage should be reasonably adjusted to obtain a larger output power. The irreversible loss mechanisms in the interelectrode space, such as the space charge effect, play a key role in the optimal design of thermionic emission devices. The space charge effect will result in an extra energy barrier and prevent electrons

*Corresponding author. Email: sushanhe@xmu.edu.cn
© 2023 Chinese Physical Society and IOP Publishing Ltd

from moving forward. As a result, both the net electron current and the energy conversion efficiency of TECs are suppressed.[35,36]

In this Letter, we establish a DCFC-TIG hybrid system, in which the effects of the main irreversibilities are analyzed. Choosing the power output density as an objective function, we try to determine the optimal ranges of the key parameters. It is expected that the results obtained are of interest for readers in the research fields of waste heat recovery of fuel cells.

System Description. Figure 1 schematically shows the proposed hybrid system composed of a DCFC, a TIG, and a regenerator. The DCFC mainly consists of three parts: a packed bed anode, a lithium doped NiO cathode, and a Li_2CO_3/K_2CO_3 eutectic melt electrolyte. At the steady states, the DCFC electrochemically converts the chemical energy of carbon and oxygen into electrical power P_D and waste heat at temperature T, i.e., $C + O_2 \rightarrow CO_2 + P_D + \text{heat}$. The heat produced in the DCFC can be divided into three parts: q_{re} is carried by the products of the DCFC to preheat the reactants through the regenerator, q_L is directly dissipated into the ambient at temperature T_a as the heat loss, and q_1 is absorbed by the cathode of the TIG at temperature T_1 to generate electrical power P_T. Thereafter, the TIG releases the remaining heat q_2 to the ambient from the anode at temperature T_2. In this way, the waste heat released by the DCFC can be efficiently utilized by the TIG to export an additional power. Synthesizing each kind of subsystem, a better performance can be achieved.

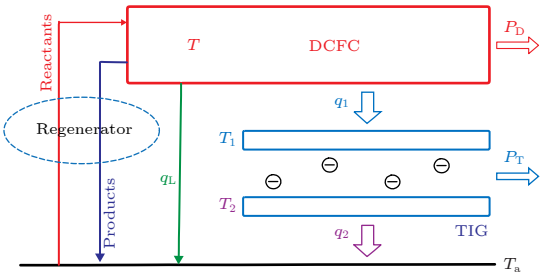

Fig. 1. A schematic drawing of the DCFC-TIG hybrid system.

As described in Fig. 1, the part of the heat directly dissipated to the environment as heat loss via convection and/or conduction can be expressed as[37]

$$q_L = (2A_D - A_T)K_L(T - T_a), \tag{1}$$

where K_L is the convective and/or conductive heat-leak coefficient, A_D is the effective electrode area of the DCFC, and A_T is the effective electrode area of the TIG.

To simplify our model, the following assumptions are adopted:[24,32,38] (1) The DCFC-TIG hybrid system is discussed in the case of steady states, and the cathode temperature of the TIG is identical to that of the DCFC. (2) Completing oxidation of carbon to CO_2 will be adopted in our model.[26] (3) The length of the vacuum gap inside the TIG is several micrometers, in which the space charge effect can be ignored. (4) The anode temperature of the TIG is also kept constant, and the electrodes of the TIG have the same inside area. Based on the above simplifications and assumptions, the performance characteristics of the subsystems and hybrid system will be synthetically investigated.

Power Output and Efficiency of a DCFC. The DCFC mainly consists of two electrodes and a sandwiched electrolyte. When the carbon and oxygen are supplied to the anode and cathode, the electrons are continuously driven from the anode to the cathode through the external circuit and an electric current I_D is produced. The enthalpy change per unit time for the electrochemical reaction can be described as $-\Delta\dot{H} = -\Delta h^0 j_D A_D/(n_e F)$, where $-\Delta h^0$ is the standard molar enthalpy change which can be calculated by the data in Ref. [26], j_D is the current density of the DCFC, $n_e = 4$ is the number of electrons transferred per graphite molecule, and $F = 96485\,\text{C/mol}$ is Faraday's constant. Using the Nernst equation, the open circuit voltage E with specific gas concentration at operating temperature T is expressed as

$$E = -\frac{1}{n_e F}\left[\Delta g^0(T) - RT\ln\left(\frac{p_{O_2,\,cat}\,p^2_{CO_2,\,cat}}{p_{CO_2,\,an}}\right)\right], \tag{2}$$

where $\Delta g^0(T)$ is the Gibbs free energy change at $p_0 = 1\text{atm}$, R is the universal gas constant, and p_{CO_2} and p_{O_2} are, respectively, the pressures of CO_2 and O_2 at the surfaces of the anode or cathode, which are denoted by the subscripts an or cat.

Considering the electrode kinetics, the reactants/products transportation, and the electronic/ionic resistances of the cell components, the output voltage, power output, and efficiency of a practical DCFC can be, respectively, written as[12,24,39]

$$\begin{aligned} V_D &= E - V_{act} - V_{con} - V_{ohm} \\ &= -\frac{RT}{n_e F}\left\{\frac{\Delta g^0(T)}{RT} + \frac{n_e}{2}\ln(a_2 a_3) \right. \\ &\quad \left. + \ln\left[\frac{j_{lim}}{a_1(j_{lim} - j_D)}\right]\right\} - V_{ohm}, \end{aligned} \tag{3}$$

$$P_D = A_D j_D V_D, \tag{4}$$

$$\eta_D = -n_e F V_D/\Delta h^0, \tag{5}$$

where $a_1 = p_{O_2,cat}p^2_{CO_2,cat}/p_{CO_2,an}$, $a_2 = j_D/(2j_{0,\,an}) + \sqrt{[j_D/(2j_{0,\,an})]^2 + 1}$, and $a_3 = j_D/(2j_{0,\,cat}) + \sqrt{[j_D/(2j_{0,\,cat})]^2 + 1}$; $j_{0,an} = K_B\exp(-E_B/T)$ and $j_{0,cat} = j^0_{0,cat}(p_{CO_2,\,cat})^{-1.250}(p_{O_2,\,cat})^{0.375}$ are the exchange currents' densities; $j_{lim} = n_e F K_{CO_2} C^b_{CO_2}$ is the limiting current density, $C^b_{CO_2}$ is the concentration of CO_2 in the bulk material, and K_{CO_2} is the mass transportation coefficient of CO_2. The specific expressions of the overpotentials in Eq. (3) as functions of j_D can be written as[12,14,26]

$$V_{act,an} = \frac{RT}{2F}\ln\left\{\frac{j_D}{2j_{0,an}} + \sqrt{[j_D/(2j_{0,\,an})]^2 + 1}\right\}, \tag{6}$$

$$V_{act,cat} = \frac{RT}{2F}\ln\left\{\frac{j_D}{2j_{0,cat}} + \sqrt{[j_D/(2j_{0,\,cat})]^2 + 1}\right\}, \tag{7}$$

$$V_{con} = \frac{RT}{n_e F}\ln[j_{lim}/(j_{lim} - j_D)], \tag{8}$$

$$V_{ohm} = \sum I_{e,i}R_{e,i} + \sum I_{c,i}R_{c,i} + V_{ec}. \tag{9}$$

Here, $I_{e,i}$ and $I_{c,i}$ are the electric currents flowing through the electrolyte and phase carbon at the ith slab in the anode, $R_{e,i}$ and $R_{c,i}$ are the corresponding resistances, and V_{ec} is the total ohmic overpotential in the electrolyte and the cathode. The total ohmic overpotential can be calculated by the method in Ref. [26].

Regenerator. Generally, the inlet reactants can be sufficiently preheated by using the energy from the outlet gas of the fuel cell through a regenerator, as shown in Fig. 1. While the non-ideal regenerative process is considered, the additional heat loss should be supplied by the waste heat of the fuel cell, which is assumed to be proportional to the temperature difference between the DCFC and the ambient, i.e.,

$$q_{re} = A_{re}K_{re}(T - T_a), \tag{10}$$

where A_{re} and K_{re} are the effective heat-transfer area and coefficient, respectively.

Power Output and Efficiency of a TIG. A typical TIG is composed of two parallel metal electrodes with unique temperatures and work functions, and separated by a micron-scale vacuum gap. When the system is normally operated, the cathode of the TIG absorbs the waste q_1 resulting in electrons emitting from the cathode surface. Meanwhile, the reverse electrons are excited from the anode. The net electrical current density of the two electrodes can be described by the Richardson equation,[40,41] i.e.,

$$j_T = j_{T,1} - j_{T,2}, \tag{11}$$

where $j_{T,1} = A_0T^2\exp[-e(\Phi_2 + V_T)/(k_BT)]$ and $j_{T,2} = A_0T_2^2\exp[-e\Phi_2/(k_BT_2)]$ are, respectively, the electronic current density of the cathode and the anode, e represents the fundamental electronic charge, A_0 is the Richardson–Dushman constant, Φ_2 is the work function of the anode, $V_T = \Phi_1 - \Phi_2$ is the operating voltage of the TIG, Φ_1 is the work function of the cathode, and k_B is the Boltzmann constant. Accompanying the electron transportation, a part of the heat can be taken by the electrons. By considering the heat loss between the two electrodes, the net heat flux densities absorbed by the cathode and released to the ambient by the anode can be, respectively, expressed as

$$\frac{q_1}{A_T} = (V_T + \Phi_2)j_T + \frac{2k_B}{e}(Tj_{T,1} - T_2j_{T,2}) + \varepsilon_T\sigma(T^4 - T_2^4), \tag{12}$$

$$\frac{q_2}{A_T} = \Phi_2 j_T + \frac{2k_B}{e}(Tj_{T,1} - T_2j_{T,2}) + \varepsilon_T\sigma(T^4 - T_2^4), \tag{13}$$

where ε_T is the thermal emissivity of the inner surfaces of the electrodes and σ is the Stefan–Boltzmann constant. Based on Eqs. (12) and (13), the power output and efficiency of the TIG can be derived as

$$P_T = q_1 - q_2 = A_TV_TA_0T^2\Big\{\exp\Big[-\frac{e(\Phi_2 + V_T)}{k_BT}\Big] - \Big(\frac{T_2}{T}\Big)^2\exp\Big[-\frac{e\Phi_2}{k_BT_2}\Big]\Big\}, \tag{14}$$

$$\eta_T = \frac{P_T}{q_1}. \tag{15}$$

Power and Efficiency of the Hybrid Systems. By using Eqs. (4), (5), (14), and (15), the power output density and efficiency of the hybrid system can be derived as

$$\begin{aligned} P_s^* &= \frac{P_D + P_T}{A_D} \\ &= -\frac{j_DRT}{n_eF}\Big\{\frac{\Delta g^0(T)}{RT} + \frac{n_e}{2}\ln(a_2a_3) + \ln\Big[\frac{j_{lim}}{a_1(j_{lim} - j_D)}\Big]\Big\} - A_Dj_DV_{ohm} \\ &\quad + \lambda V_TA_0T^2\Big\{\exp\Big[-\frac{e(\Phi_2 + V_T)}{k_BT}\Big] - \Big(\frac{T_2}{T}\Big)^2\exp\Big[-\frac{e\Phi_2}{k_BT_2}\Big]\Big\}, \end{aligned} \tag{16}$$

$$\begin{aligned} \eta_s &= \frac{P_D + P_T}{-\Delta\dot{H}} \\ &= \eta_D + \lambda\eta_T\Big\{1 + \frac{1}{\Delta h^0}[(2 - \lambda)K_L + c_1](T - T_a)\Big\}, \end{aligned} \tag{17}$$

where $\lambda = A_T/A_D$ and $c_1 = A_{re}K_{re}/A_D$.

According to the first law of thermodynamics and Eqs. (1), (4), (10), and (12), i.e., $-\Delta\dot{H} - P_D - q_L - q_{re} - q_1 = 0$, the area ratio λ can be expressed as

$$\begin{aligned} \lambda = \Big[&-\frac{j_D\Delta h^0}{n_eF}(1 - \eta_{DCFC}) - (c_1 + 2K_L)(T - T_a)\Big] \\ &\cdot\Big\{[(V_T + \Phi_2)j_T + \frac{2k_B}{e}(Tj_{T,1} - T_2j_{T,2}) \\ &+ \varepsilon_T\sigma(T^4 - T_2^4)] - K_L(T - T_a)\Big\}^{-1}. \end{aligned} \tag{18}$$

For the DCFC operating at a fixed temperature, the operating condition of the DCFC should satisfy the following condition so that the TIG starts to work,

$$j_D(1 - \eta_D) > -\frac{n_eF}{\Delta h}(c_1 + 2K_L)(T - T_a). \tag{19}$$

According to Eq. (18) and the parameters in Table 1, the graph of the area ratio as a function of the current density of the DCFC and the voltage of the TIG can be plotted, as shown in Fig. 2(a). Unless mentioned otherwise, the parameters in Fig. 2 are used in the following discussion. The dotted line j_C in Fig. 2(a) denotes the cut-off current density, which can be directly calculated by Eq. (18). Clearly, λ monotonically increases with either the current density or voltage. It is seen from Eq. (12) that for a given voltage, the heat flux density q_1/A_T is fixed. The rising current density of the DCFC results in more waste heat. As a result, the value of λ increases. In Fig. 2(b), with the increase of V_T, the heat flux density q_1/A_T monotonically decreases. Thus, when the value of j_D is fixed, the area of the TIG increases to sufficiently absorb the waste heat from the DCFC.

Table 1. Operation parameters of the DCFC-TIG system.[26,30]

Parameter	Value
Concentration independent cathode exchange current density, $j^0_{0,\mathrm{cat}}$ (A/m^2)	5.0×10^2
Pre-exponential factor of the backward reaction, K_B (A/m^2)	5.8×10^9
Temperature activation of the backward reaction, E_B (K^{-1})	2.2×10^4
Mass transport coefficient of CO_2, K_{CO_2} (m/s)	3.5×10^{-2}
Compositions pressure at the cathode side, p_{CO_2}, p_{O_2}	0.67, 0.33
Operating pressure, p (Pa)	1.013×10^5
Faraday constant, F (C/mol)	96485
Universal gas constant, R [J/(mol · K)]	8.314
Operating temperature of DCFC, T (K)	1073
Temperature of environment, T_0 (K)	298
Quantity of electric charge, e (C)	1.6×10^{-19}
Thermal emissivity, ε_T	0.18[31]
Stefan-Boltzmann constant, σ [W/(cm^2 · K^4)]	5.67×10^{12}
Boltzmann constant, k_B (J/K)	1.38×10^{-23}
Work function of the anode of the TIG, Φ_2 (eV)	1.2
Temperature of the anode of the TIG, T_2 (K)	500
Standard molar enthalpy change at 1073 K, 1023 K, 973 K, 923 K, Δh^0 (10^5 J/mol)	−3.4239, −3.4425, −3.4621, −3.4827
Standard molar Gibbs free energy change at 1073 K, 1023 K, 973 K, 923 K, Δg^0 (10^5 J/mol)	−3.3819, −3.4054, −3.4298, −3.4553

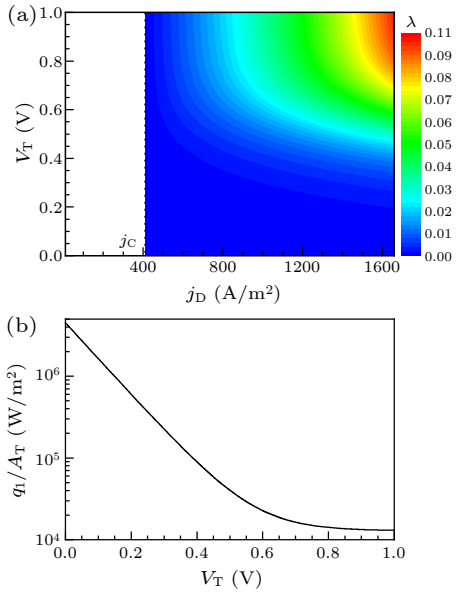

Fig. 2. (a) The area ratio as a function of the current density of the DCFC, (b) the heat flux density absorbed by the cathode of the TIG as a function of the voltage of the TIG, where $c_1 = 0.1\,\mathrm{W/(m^2 \cdot K)}$, $K_\mathrm{L} = 0.05\,\mathrm{W/(m^2 \cdot K)}$, and other parameters are listed in Table 1.

Results and Discussion. By using Eqs. (4), (5), and (15)–(17), the contour graphs of the power output density P_s^* and efficiency η_s of the hybrid system as functions of V_T and j_D are shown in Fig. 3(a) and 3(b). When $j_\mathrm{D} \leqslant j_\mathrm{C}$, the values of P_s^* and η_s are equal to those of the DCFC described by Eqs. (4) and (5). When $j_\mathrm{D} > j_\mathrm{C}$, the TIG starts to work, and P_s^* and η_s are, respectively, described by Eqs. (16) and (17). It can be seen from Fig. 3(a) that the power output density of the hybrid system is not a monotonic function of V_T and j_D, with a maximum value $P^*_{\mathrm{s,m}}$, where V_opt and j_opt are the corresponding optimal values. When $V_\mathrm{opt} = 0.42\mathrm{V}$ and $j_\mathrm{opt} = 1100\mathrm{A/m^2}$, the maximum power output density $P^*_{\mathrm{s,m}} = 349.07\mathrm{W/m^2}$ can be attained. In Fig. 3(b), it is seen that η_s monotonically decreases with the increase of the current density of the DCFC. It should be pointed out that the existence of the TIG slows down the decreasing speed of the efficiency. For a given j_D, the η_s increases firstly and then decreases by increasing V_T, which can be concluded from Eq. (14). When $V_\mathrm{T} = 0$ and $V_\mathrm{T} = (T/T_2 - 1)\Phi_2 + (2k_\mathrm{B}T/e)\ln(T/T_2)$, the power output of the TIG $P_\mathrm{T} = 0$.

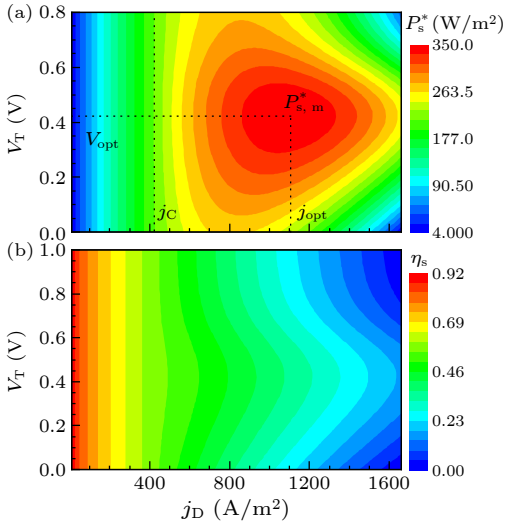

Fig. 3. Contour graphs of (a) the power output density and (b) the efficiency of the DCFC-TIG system as functions of V_T and j_D.

By using Eq. (16) and the extremal condition $\partial P_\mathrm{s}/\partial V_\mathrm{T} = 0$, we can draw the curves of the power output densities of the hybrid system, DCFC and TIG varying with the DCFC's current density, as shown in Fig. 4.

Comparing the solid and dashed lines, one can see that when $j_{\rm D} > j_{\rm C}$ the power density of the hybrid system is larger than that of the DCFC. In Fig. 4, $j_{\rm D,opt}$ indicates the current density at the maximum power point $P_{\rm D,m}/A_{\rm D}$ of the DCFC, while $j_{\rm L}$ and $j_{\rm U}$ are obtained from the condition that $P_{\rm s} = P_{\rm D,m}$. We can conclude from the operating boundaries of the current density that the performances of the hybrid system are better than those of the DCFC, i.e.,

$$j_{\rm L} \leqslant j_{\rm D} \leqslant j_{\rm U}. \tag{20}$$

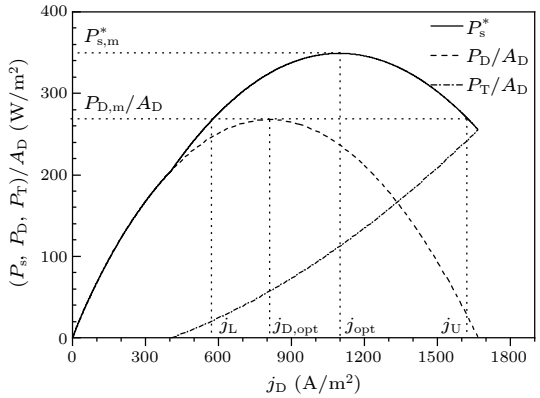

Fig. 4. Power output densities of the DCFC (dashed line), TIG (dash dotted line), and hybrid system (solid line) against the current density of the DCFC, where the voltage has been optimized.

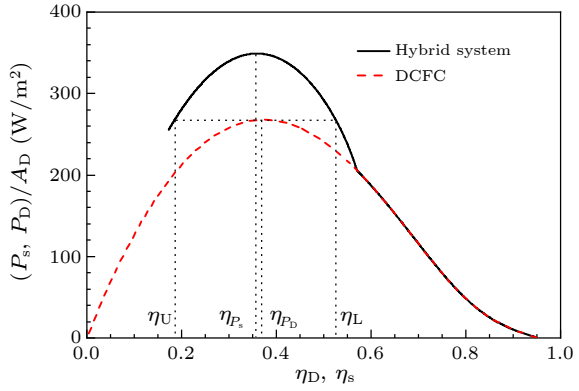

Fig. 5. Performance characteristic curves of the DCFC (dashed line) and DCFC-TIG hybrid system (solid line).

According to Eqs. (4), (5), (16), (17), and the extremal condition $\partial P_{\rm s}/\partial V_{\rm T} = 0$, one can obtain the power output density as a function of the efficiency, as shown in Fig. 5, where $\eta_{P_{\rm s}}$ and $\eta_{P_{\rm D}}$ are the efficiencies at the maximum power outputs of the hybrid system and DCFC, respectively. Similarly, by considering the condition that $P_{\rm s} \geqslant P_{\rm D,m}$, the efficiency should satisfy the relation

$$\eta_{\rm U} \leqslant \eta_{\rm s} \leqslant \eta_{\rm L}, \tag{21}$$

where the value of $\eta_{\rm U}$ (or $\eta_{\rm L}$) can be obtained from the data in Fig. 4 and Eq. (17) for $j_{\rm D} = j_{\rm U}$ (or $j_{\rm L}$).

In Fig. 6, the influence of the anode work function of the TIG on the boundary condition in Eq. (20) is revealed. The dash-dotted line indicates the optimal values of $V_{\rm T}$ (or $j_{\rm D}$) for the given values of $j_{\rm D}$ (or $V_{\rm T}$) to achieve the maxima of the power output density of the DCFC-TIG system for $\Phi_2 = 1.2\,{\rm eV}$. The cross point of the dashed lines denotes the maximum power. It is clearly seen that both the DCFC's current density and the TIG's voltage have boundaries so that the hybrid system always performs better than the DCFC, which can be written as Eq. (20), and

$$V_{\rm L} \leqslant V_{\rm T} \leqslant V_{\rm U}. \tag{22}$$

Clearly, the area inside the boundaries increases with the decrease of the work function of the TIG.

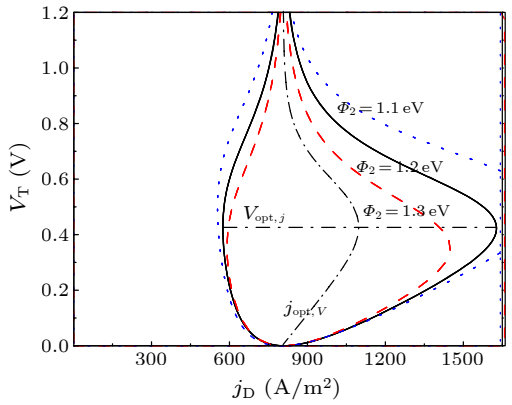

Fig. 6. Influence of the work function of the TIG on the boundary in Eq. (20), where $j_{{\rm opt},V}$ ($V_{{\rm opt},j}$) are the optimal values under the condition that $V_{\rm T}$ ($j_{\rm D}$) is given.

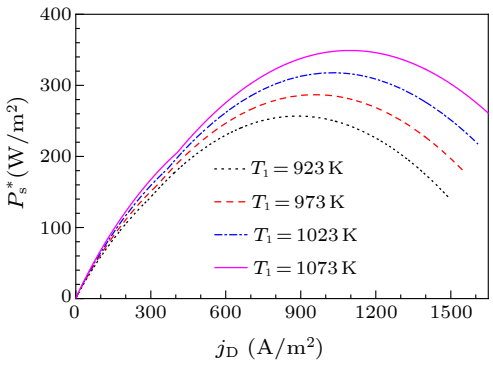

Fig. 7. Influence of the operation temperature of the DCFC on the power output density of the hybrid system.

In addition, the influence of the operating temperature on the power output density of the hybrid system is graphically revealed in Fig. 7. It is seen from Fig. 7 that the higher the operating temperature, the larger the current density range and the power output density.

Using Eq. (16), we calculate the maximum power output density of the hybrid system for given values of Φ_2 and T, and the optimal values of the main parameters under the maximum power output density condition, as listed in Table 2. In the last line, the values of $(P_{\rm s,\,m} - P_{\rm D,\,m})/P_{\rm D,m}$ are indicated. Clearly, the DCFC's power density can be boosted by 41% for $\Phi_2 = 1.1\,{\rm eV}$ and $T = 1073\,{\rm K}$. The maximum power of the DCFC is efficiently enhanced by the hybrid system.

Table 2. The optimal values of the other main parameters under the maximum power output density condition.

Φ_2 (eV)	1.3			1.2			1.1		
T (K)	1073	1023	973	1073	1023	973	1073	1023	973
$P_{\rm s}^{*}$ (10^{-2} W/m^2)	3.25	2.95	2.66	3.49	3.18	2.87	3.79	3.46	3.13
$\eta_{\rm P}$	0.36	0.35	0.33	0.36	0.35	0.33	0.36	0.35	0.33
$j_{\rm opt}$ (10^{-2} A/m^2)	10.18	9.53	8.88	10.97	10.27	9.57	11.91	11.17	10.43
$V_{\rm opt}$ (V)	0.35	0.30	0.25	0.42	0.37	0.31	0.50	0.44	0.38
$j_{\rm L}$ (10^{-2} A/m^2)	5.92	5.72	5.55	5.74	5.52	5.30	5.61	5.35	5.11
$j_{\rm U}$ (10^{-2} A/m^2)	14.52	13.40	12.25	16.29	15.10	13.91			
$V_{\rm L}$ (V)	0	0	0	0	0	0	0	0	0
$V_{\rm U}$ (V)	1.63	1.49	1.34	1.16	1.19	1.25	1.40	1.28	1.15
$\eta_{\rm L}$	0.51	0.49	0.46	0.53	0.51	0.48	0.54	0.52	0.50
$\eta_{\rm U}$	0.21	0.21	0.21	0.19	0.18	0.18			
$(P_{\rm s,\,m} - P_{\rm D,\,m})/P_{\rm D,m}$	0.22	0.19	0.16	0.30	0.28	0.25	0.41	0.39	0.37

In summary, we have proposed a hybrid system consisting of a direct carbon fuel cell, a thermionic generator, and a regenerator. The analytical expressions of the power output and efficiency of the subsystems and hybrid system have been derived. The area matching problem between the DCFC and TIG has been discussed in detail. The maximum power output density and the corresponding efficiency are calculated. The corresponding optimal values of the current density of the DCFC and the voltage of the TIG are also obtained. The reasonable regions of other key parameters are also determined to enhance the maximum power density of the DCFC, in which the power output of the hybrid system is larger than that of either subsystem. The results show that the waste heat produced in high temperature fuel cells can be efficiently utilized and is worthy to be further studied.

Acknowledgment. This research was supported by Programs for Tackling Key Problems in Science and Technology of Henan Province (Grant No. 222102240004).

References

[1] Cao D, Sun Y, and Wang G 2007 *J. Power Sources* **167** 250
[2] Xu Q D, Guo Z J, Xia L C, He Q J, Li Z, Bello I T, Zheng K Q, and Ni M 2022 *Energy Conver. Manag.* **253** 115175
[3] Jiang C R, Ma J J, Corre G, Jain S L, and Irvine J T S 2017 *Chem. Soc. Rev.* **46** 2889
[4] İnci M 2022 *Sustain. Energy Technol. Assess.* **53** 102739
[5] Liu R Z, Zhao C H, Li J L, Zeng F R, Wang S R, Wen T L, and Wen Z Y 2010 *J. Power Sources* **195** 480
[6] Li C, Shi Y X, and Cai N S 2011 *J. Power Sources* **196** 754
[7] Xie Y M, Tang Y B, and Liu J 2013 *J. Solid State Electrochem.* **17** 121
[8] Elleuch A, Boussetta A, and Halouani K 2012 *J. Electroanal. Chem.* **668** 99
[9] Hemmes K, Houwing M, and Woudstra N 2010 *J. Fuel Cell Sci. Technol.* **7** 051008
[10] Kacprzak A, Kobylecki R, and Bis Z 2013 *J. Power Sources* **239** 409
[11] Nunoura T, Dowaki K, Fushimi C, Allen S, Mészáros E, and Antal M J 2007 *Ind. Eng. Chem. Res.* **46** 734
[12] Giddey S, Badwal S P S, Kulkarni A, and Munnings C 2012 *Prog. Energy Combust. Sci.* **38** 360
[13] Vutetakis D G, Skidmore D R, and Byker H J 1987 *J. Electrochem. Soc.* **134** 3027
[14] Cherepy N J, Krueger R, Fiet K J, Jankowski A F, and Cooper J F 2005 *J. Electrochem. Soc.* **152** A80
[15] Watanabe H, Kimura A, and Okazaki K 2016 *Energy Fuels* **30** 1835
[16] Kulkarni A, Ciacchi F T, Giddey S, Munnings C, Badwal S P S, Kimpton J A, and Fini D 2012 *Int. J. Hydrogen Energy* **37** 19092
[17] Giddey S, Kulkarni A, Munnings C, and Badwal S P S 2014 *Energy* **68** 538
[18] Kulkarni A, Giddey S, and Badwal S P S 2011 *Solid State Ionics* **194** 46
[19] Xu H R, Chen B, Zhang H C, Tan P, Yang G M, Irvine J T S, and Ni M 2018 *J. Power Sources* **382** 135
[20] Xu H R, Chen B, Tan P, Zhang H C, Yuan J L, Irvine J T S, and Ni M 2018 *Energy Conver. Manag.* **165** 761
[21] Xu H R, Chen B, Tan P, Cai W Z, Wu Y Y, Zhang H C, and Ni M 2018 *Appl. Energy* **226** 881
[22] Liu Q H, Tian Y, Xia C, Thompson L T, Liang B, and Li Y D 2008 *J. Power Sources* **185** 1022
[23] Eom S, Ahn S, Kang K, and Choi G 2017 *J. Power Sources* **372** 54
[24] Xu H R, Chen B, Zhang H C, Sun Q, Yang G M, and Ni M 2017 *Int. J. Hydrogen Energy* **42** 15641
[25] Steinberg M 2006 *Int. J. Hydrogen Energy* **31** 405
[26] Zhang H C, Chen L W, Zhang J J, and Chen J C2014 *Energy* **68** 292
[27] Dimitrova Z and Maréchal F 2017 *Renewable Energy* **112** 124
[28] Bellomare F and Rokni M 2013 *Renewable Energy* **55** 490
[29] Wang R Z, Li G Q, Ma Y Y, Wang T P, Chen B, Wei T, and Dong D H 2023 *Int. J. Hydrogen Energy* **48** 9797
[30] Wang Y, Su S H, Lin B H, and Chen J C 2013 *J. Appl. Phys.* **114** 053502
[31] Wang Y, Cai L, Liu T, Wang J, and Chen J 2015 *Energy* **93 Part 1** 900
[32] Huang C K, Pan Y Z, Wang Y, Su G Z, and Chen J C 2016 *Energy Conver. Manag.* **121** 186
[33] Abraham K and Gideon S 2016 *J. Opt.* **18** 073001
[34] Olawole O C and De D K 2018 *J. Photon. Energy* **8** 018001
[35] Zhang P, Ang Y S, Garner A L, Valfells Á, Luginsland J W, and Ang L K 2021 *J. Appl. Phys.* **129** 100902
[36] Zhang P, Valfells Á, Ang L K, Luginsland J W, and Lau Y Y 2017 *Appl. Phys. Rev.* **4** 011304
[37] Zhang H, Xu H, Chen B, Dong F, and Ni M 2017 *Energy* **132** 280
[38] Khalid K A A, Leong T J, and Mohamed K 2016 *IEEE Trans. Electron. Devices* **63** 2231
[39] Zhao M, Zhang H, Hu Z, Zhang Z, and Zhang J 2015 *Energy Conver. Manag.* **89** 683
[40] Dushman S 1923 *Phys. Rev.* **21** 623
[41] Richardson O W 1912 *Dublin Philos. Mag. J. Sci.* **23** 594